



Step-Growth Thiol-Thiol Photopolymerization as Radiation Curing Technology

Noémi Feillée, Maurizio de Fina, Arnaud Ponche, Cyril Vaultot, Séverinne Rigolet, Leandro Jacomine, Hicham Majjad, Christian Ley, Abraham Chemtob

► To cite this version:

Noémi Feillée, Maurizio de Fina, Arnaud Ponche, Cyril Vaultot, Séverinne Rigolet, et al.. Step-Growth Thiol-Thiol Photopolymerization as Radiation Curing Technology. *Journal of Polymer Science Part A: Polymer Chemistry*, 2017, 55 (1), pp.117-128. <10.1002/pola.28369>. <hal-02442158>

HAL Id: hal-02442158

<https://hal.science/hal-02442158v1>

Submitted on 16 Jan 2020

HAL is a multi-disciplinary open access archive for the deposit and dissemination of scientific research documents, whether they are published or not. The documents may come from teaching and research institutions in France or abroad, or from public or private research centers.

L'archive ouverte pluridisciplinaire **HAL**, est destinée au dépôt et à la diffusion de documents scientifiques de niveau recherche, publiés ou non, émanant des établissements d'enseignement et de recherche français ou étrangers, des laboratoires publics ou privés.



HAL Authorization

Step-Growth Thiol-Thiol Photopolymerization as Radiation Curing Technology

Noémi Feillée,¹ Maurizio De Fina,¹ Arnaud Ponche,² Cyril Vaultot,² Séverinne Rigolet,² Leandro Jacomine,³ Hicham Majjad,⁴ Christian Ley,^{*1} Abraham Chemtob^{*2}

¹ Laboratory of Macromolecular Photochemistry and Engineering, University of Haute-Alsace, EA 4567, 3 rue Alfred Werner, 68093 Mulhouse Cedex, France.

² Institute of Mulhouse Material Science, University of Haute-Alsace, UMR-CNRS 7361, 15 rue Jean Starcky, 68057 Mulhouse Cedex, France.

³ Institute Charles Sadron, University of Strasbourg, UPR-CNRS 22, 23 rue du Loess, BP 84047, 67034 Strasbourg Cedex 2, France

⁴ Institute of Material Chemistry and Physics of Strasbourg, University of Strasbourg, UMR-CNRS 7504, 23 rue du Loess, BP 43, 67034 Strasbourg Cedex 2, France

*Correspondence to: Abraham Chemtob (E-mail: abraham.chemtob@uha.fr)

Additional Supporting Information may be found in the online version of this article.

ABSTRACT

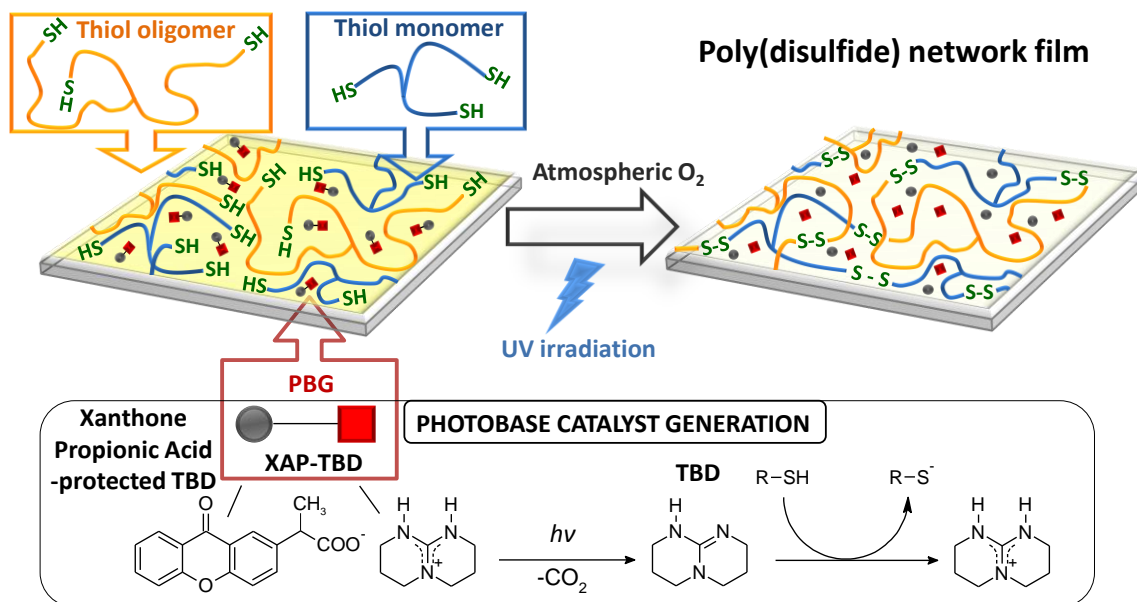
This report introduces a novel UV-curing technology based on thiol-thiol coupling for polydisulfide network formation. Beginning with a model tris(3-mercaptopropionate) trithiol monomer and xanthone propionic acid-protected guanidine as photobase generator, a comprehensive characterization based on spectroscopic techniques supports the reaction of thiols into disulfides without side reactions. The best experimental conditions are described as regards to film thickness, irradiance, emission wavelength, and atmosphere composition. The results shed light on a step-growth photopolymerization mechanism involving two steps: first, the formation of thiyl radicals by thiolate air oxidation or/and thiol photolysis, and second, their recombination into disulfide. By varying thiol functionality and structure, oligomer chain length and monomer/oligomer ratio, the network architecture can be finely tuned. The molecular mobility of the polydisulfide network is crucial to high thiol conversion rates and yields as revealed by ¹H T₂ NMR relaxation measurements. Ultimately, spatial control enables the formation of a photopatterned poly(disulfide)s film, used as next-generation high refractive index photoresist.

KEYWORDS: photopolymerization, polysulfide, step-growth polymerization, photobase generator, ultra-violet

INTRODUCTION

Radiation curing is a rapidly growing technology, primarily applied to large-scale production of polymer films for industrial coatings, graphic arts and electronic materials.¹ Ultraviolet (UV) and visible light radiation are currently the two pillars through a set of unique technical and environmental advantages: temporal and spatial control of polymerization, energy-efficient and room-temperature curing,

solvent-free and stable photocurable formulation. This latter contains generally a mixture of multifunctional monomers, oligomers and a photoinitiator, which is the key component to control the photochemical process. In this area, the biggest share goes to radical photoinitiators accounting for more than 95 % of all photopolymerizations performed in industry. These developments were achieved despite two major challenges: the restricted choice of reactive and affordable resins –



Scheme 1. UV-curing technology based on polythiol monomers and oligomers step-growth photopolymerization into disulfide polymer network via a photobase-catalyzed route.

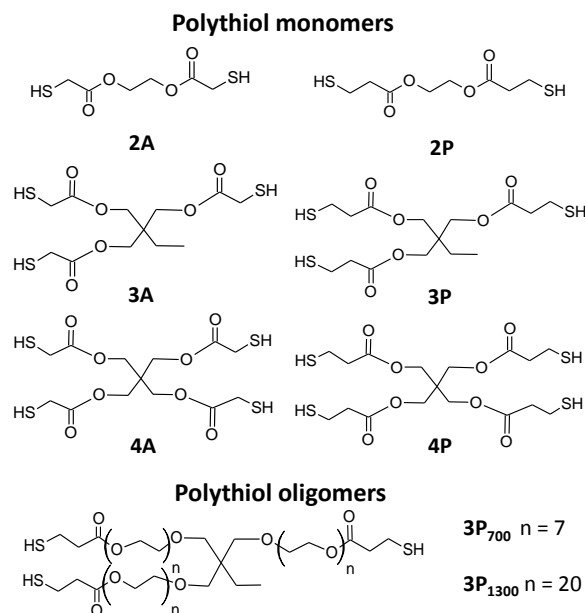
principally of acrylate type – and atmospheric oxygen's inhibition susceptible to affect film preparation and final properties. To overcome these limitations, photoacid generator (PAG) represents today one of the main alternatives, and the most emblematic are certainly Crivello's diaryliodonium and triarylsulfonium salts² able to initiate cationic polymerizations. Much less advanced technologically than the two previous systems, photobase generator (PBG) holds potential for even greater positive impacts in photopolymerization. The ascent of photolatent catalytic systems able to release strong enough Brønsted bases ($pK_a > 10$ –12) could be very beneficial for the anionic chain-growth polymerization of a broad range of monomers – e.g. acrylics, epoxides, lactones, lactams – but also suitable to organocatalyzed step-growth polymerizations such as polyurethane synthesis.³ To date, typical PBGs liberate primary, secondary or tertiary amines upon irradiation which are generally too weak catalysts for these latter reactions to be quantitative and carried out at high rates.⁴

In recent years, attention has been directed at designing PBGs able to release organosuperbases, especially carboxamidines

$RC(=NR)NR_2$ which boast a pK_a value 3–4 orders of magnitude greater than tertiary amines.⁵ The main examples are 1,1,3,3-tetramethylguanidine (TMG), 1,5-diazabicyclo[4.3.0] non-5-ene (DBN) or 1,5,7-triazabicyclo[4.4.0]dec-5-ene (TBD). To obtain these various catalysts in a photolatent form, the main strategy has consisted in protecting the strong bases with a light-responsive group including coumarin,⁶ ketoprofen and xanthone acetic acid,⁷ phenylglyoxylic acid,⁸ tetraphenylborate,^{9, 10} or nitrophenyl propyl.¹¹ Because of their inherent high Brønsted-basicity, photogenerated amidines have already showed efficiency in several cross-linking reactions, including thiol-epoxy,⁷ thiol-Michael,^{6, 9, 11} malonate Michael,¹² or epoxy ring-opening.^{8, 10} These few examples give a first glimpse on the potential of amidine-mediated photopolymerizations. We have recently extended the scope to thiol air oxidation to form polydisulfide network films¹³ in presence of a xanthone propionic acid-protected TBD (**XAP-TBD**).⁷ Thiols (RSH) are generally mild acids ($pK_a = 5$ –11)¹⁴ meaning that a guanidine derivative such as TBD ($pK_a \approx 13.5$) can deprotonate most thiols to form a thiolate

anions RS^- acting as a much stronger nucleophile. This shift enables reaction with mild oxidants such as oxygen to form thiyl radicals (RS^\bullet), and subsequent dimerization of the radicals to the disulfide ($RS-SR$). Important in living organisms involving sulfur-containing amino acids and proteins, the (non-latent) oxidation of thiol to disulfide is also a well-established industrial process for curing liquid thiol-terminated oligomers.^{15, 16} The resulting disulfide polymer specialty elastomers, often referred to as Thiokols®, derive their utility from their good solvent and environmental resistance, and low-temperature properties. Used mainly as hose, gaskets, sealants for insulating glass or fuel tanks, the curing process occurs at ambient temperature in a few hours in presence of oxidizing agent in addition to oxygen.

This report lays the foundation for a novel UV-curing technology based on thiol-thiol photocoupling into disulfide. The challenge is to create a new range of disulfide-containing UV-curable coatings at high rates (in the order of sec) and in solvent-free conditions using a portfolio of commercial thiol-terminated monomers and oligomers, as depicted in **Scheme 1**. In contrast to conventional radical and cationic UV-curing, the network construction proceeds by step-growth polymerization, which stands out by the fact that two similar SH functional groups react together to form a disulfide bond. Important for optimizing light penetration, a thin film thickness becomes also essential for air permeation and atmospheric oxygen oxidation, thus avoiding the need of external oxidizing agent (manganese oxide, sodium perborate...). Therefore, the step-growth air photopolymerization of a single thiol monomer A_f with a functionality $f \geq 3$ may result in the formation of a cross-linked high sulfur content polydisulfide network. Outstanding properties are often associated to polymer containing a high content of S-S bonds in their backbone such as higher chemical resistance,¹⁷ water vapor impermeability,¹⁸ high refractive index,¹⁹



Scheme 2. List of multifunctional thiol derivatives **xA** or **xP**, with **x** the thiol functionality, while **A** or **P** refers to acetate thiol and propionate thiol respectively.

electrochemical activity towards lithium^{20, 21} and dynamic covalent character.^{22, 23} Recently, this latter property resulting from the reversibility of the S-S bond has found utility for applications as self-healing materials²⁴, rewritable surfaces²⁵ and drug delivery carriers.²⁶

In this report, we present extensive characterization evidences which show that multiple conversions of polythiol into polydisulfide can proceed under UV exposure in presence of **XAP-TBD** with minimal side reactions. The study of key experimental parameters establishes that thiyl radicals — leading to disulfide bonds by coupling reaction — can originate not only from a photobase-catalyzed air oxidation of thiol but also from direct thiol photolysis. Further, the step photopolymerization ability of range of thiolated monomers and oligomers (listed in **Scheme 2**) was assessed. By varying parameters such as thiol functionality (2-4) and thiol structure (acetate or propionate), oligomer chain length and monomer/oligomer ratio, the network architecture can be finely tuned. Based on 1H T_2 NMR relaxation analysis, we demonstrate that chain molecular mobility is

crucial in order to achieve fast rates and high thiol conversion. This opens the way for a new radiation curing technology based on thiols' photocoupling. Ultimately, photopatterned high sulfur content polymers were produced by conventional UV photolithography techniques, to be used as next-generation high refractive index photoresists.

EXPERIMENTAL

Materials

Ethylene glycol bis(mercaptoacetate) (**2A**, 210 g mol⁻¹), trimethylolpropane tris(3-mercaptoacetate) (**3A**, 357 g mol⁻¹), pentaerythritol tetrakis(3-mercaptoacetate) (**4A**, 433 g.mol⁻¹), ethylene glycol bis(mercaptopropionate) (**2P**, 238 g/mol), trimethylolpropane tris(3-mercaptopropionate) (**3P**, 399 g.mol⁻¹), pentaerythritol tetrakis(3-mercaptopropionate) (**4P**, 489 g.mol⁻¹), trimethylolpropane tris(3-mercaptopropionate) poly(ethylene oxide) oligomers (**3P**₇₀₀, 708 g.mol⁻¹ and **3P**₁₃₀₀, 1274 g.mol⁻¹) were provided by Bruno Bock. 2-(9-oxoxanthen-2-yl)propionic acid 1,5,7-triazabicyclo[4.4.0]dec-5-ene Salt (**XAP-TBD**) used as PBG was purchased from TCI. Chloroform (>99%) was purchased from Sigma-Aldrich. All reagents were used as received without further purification.

Synthesis of disulfide polymer films

In a typical polymerization reaction, 20 mg of PBG **XAP-TBD** was dissolved in chloroform (4 g) and 0.48 g of thiol monomer/oligomer was added. A 1.7 μ m thick film deposition was made by spin-coating (5 s at 1000 rpm then 10 s at 2000 rpm) on a KBr or glass substrate previously cleaned with technical grade acetone (≥ 99.5 wt%). Thickness was controlled by adjusting the CHCl₃ concentration and assessed by profilometry measurements (3D surface profiler Bruker).

Two UV irradiation devices were implemented for photopolymerization experiments. For RT-FTIR and Raman experiments, ambient UV

irradiation in air was performed during 900 s using a medium-pressure Hg-Xe lamp (Hamamatsu L8251, 200 W) coupled with a flexible light-guide. A total irradiance of 490 mW cm⁻² (λ =200 - 800 nm) was measured at the surface of the film sample by conventional radiometric techniques. The irradiation device is equipped with an elliptical reflector (365 nm) that efficiently reflects the UV light, and lets heat rays and visible light pass through, preventing any significant increase of temperature. Using this cold reflector cutting off heat, the local temperature during the process may be increased of ca. 3 °C. For experiments performed under nitrogen or saturated oxygen, the sample was performed in a controlled-environment chamber where atmosphere was adjusted. Light entry into the chamber was enabled by a KBr window transparent to UV light. For NMR and thermal analysis, UV exposure was carried out through ten successive passes under a UV conveyor (Qurtech) equipped with an electrodeless "H-bulb" lamp powered by microwave irradiation (Fusion). The "H-bulb" output is most similar to a conventional medium pressure mercury electrode type lamp output. The belt speed of the conveyor was set to 10 m min⁻¹. Under these conditions, the emitted light dose for each pass is 1.35 J cm⁻² (UVA [320-390 nm]: 0.46 J cm⁻², UVB [280-320 nm]: 0.31 J cm⁻², UVC [250-260 nm]: 0.08 J cm⁻² and UVV [395-445 nm]: 0.50 J cm⁻²) and corresponds to an exposure time of 0.23 s.

Characterization techniques

Confocal Raman microscopy enables the recording of Raman spectra using an in via Raman reflex microscope from Renishaw. The excitation wavelength was provided by a He-Ne laser from Renishaw emitting 17 mW cm⁻² at 633 nm. The objective used was N PLAN 50 \times Leica with a numerical aperture of 0.75. A 600 l/mm grating optimized for visible light was used to disperse the light on a CCD NIR deep depletion Peltier cooled detector camera. A 30 s exposure and a 10 spectra accumulation were

needed to obtain a reasonable signal-to-noise ratio. The conversion rate of thiol functions was determined by integration of the Raman SH stretching band at 2570 cm⁻¹ before and after irradiation. Raman mapping profiles were achieved by displacement of the optical plate holding the sample. A spectrum was taken every micrometer on a 260 µm-long line.

Real-time Fourier transform infrared (RT-FTIR) spectra were obtained with a Bruker Vertex 70 spectrophotometer equipped with a liquid nitrogen cooled mercury-cadmium-telluride (MCT) detector working in the rapid scan mode. The resolution of the spectra was 4 cm⁻¹ with an average of 4 scans s⁻¹. The conversion rate of thiol functions over time was determined by integration of the SH stretching band at 2570 cm⁻¹.²⁷

X-ray photoelectron spectrometry (XPS) analysis was carried out using a Gamdata Scienta SES 2002 X-ray photoelectron spectrometer under ultra-high vacuum ($P < 10^{-9}$ mbar). The monochromated Al K α source was operated at a current of 30 mA and 14 kV, with a 90° nominal take-off angle (angle between the sample surface and photoemission direction). During acquisition, the pass energy was set to 200 eV for high-resolution spectra. Classical Scofield sensitivity factors were used for peak fitting procedures with CASAXPS software: S2p 1.68. All line shapes used in peak fitting procedures were a mix of 30 % Gaussian and 70 % Lorentzian shapes.

¹H NMR (400 MHz) spectrum of **3P** was recorded at room temperature on a Bruker Avance 400 spectrometer equipped with 5 mm Z-gradient QNP (¹H, ¹³C, ¹⁹F, ³¹P) probe for routine spectroscopy. The chemical shifts were referenced to the residual proton signal of the solvents CHCl₃ at 7.26 ppm for ¹H.

Solid-state ¹H (I = 1/2) MAS NMR experiment was performed at room temperature on a Bruker Avance II 400 spectrometer operating at B₀ = 9.4 T (Larmor frequency ν_0 = 400.17 MHz). Single pulse experiment was recorded with a double channel 2.5 mm Bruker MAS probe, a spinning frequency of 30 kHz and a $\pi/2$ pulse duration of 2.9 µs and a 5s recycling delay. ¹H

spin lattice relaxation times (T₁) were measured with the inversion-recovery pulse sequence. Typically, 64 scans were recorded. Chemical shifts reported thereafter are relative to tetramethylsilane ¹H. The deconvolution of the experimental ¹H MAS spectrum was carried out with the DMfit software.²⁸

Low field NMR ¹H NMR relaxation experiments were performed in 10 mm NMR tubes on a Bruker Minispec MQ-20 spectrometer operating at proton resonance frequency of 20 MHz. The experiments were performed at 45°C (initial magnet temperature) under static conditions. Before performing whatever NMR analysis, Proton spin–lattice relaxation times T₁ were measured with the inversion-recovery pulse sequence,

$$\pi - \tau - \frac{\pi}{2} - \tau - acquisition$$

The measurement of the time T₁ for each materials allowed us to optimize and set the recycle delay in the following analyses. Next, Proton spin-spin relaxation times (T₂) were measured with different sequences and, in particular, by using the Free Induction Decay (FID),

$$\frac{\pi}{2} - acquisition$$

and the Carr-Purcell-Meibloom-Gill (CPMG) pulse sequence (with CYCLOPS cycling),

$$\left(\frac{\pi}{2}\right)_x - (\tau - \pi_y - \tau - acquisition)_n$$

where x and y indicate the radio-frequency phases of the pulses with angles $\pi/2$ and π , respectively, and τ is the inter-pulse spacing. τ was taken at the value of 0.05 ms for all the analyses. This time is the minimal value to prevent the T_{1ρ} effect and to limit the initial intensity loss. The CPMG decay curves were deconvoluted by using a sum of exponential functions:

$$M(t) = \sum_{i=1}^n A_i \cdot \exp\left(\frac{-t}{T_{2,i}}\right)$$

With A_i and T_{2,i}, the proportion and transverse relaxation time of the population i. FID is the simplest NMR sequence and its intensity is directly proportional to the total amount of protons in the sample. However, in this case,

the field inhomogeneities are not compensated. Unlike, the CPMG sequence removes these inhomogeneities and provides the true T_2 but involves others problems: the echo time must be relatively long to avoid the $T_{1\rho}$ effects ($\tau \geq 0.05$ ms), refocusing of only the mobile protons. In this context, we have realized the CPMG measurements on the different materials in order to obtain the T_2 relaxation times and their ^1H distribution. The difference of intensity between CPMG and FID was attributed at the solid fractions of the materials and the associated ^1H were added at the population with the lowest T_2 -CPMG population.

Thermal gravimetric analysis (TGA) was carried out with a TGA Q500 (TA Instruments) under nitrogen atmosphere (20 mL min^{-1}). 9 mg of poly(disulfide) film was placed in an open aluminum pan and heated from ambient conditions to $900\text{ }^\circ\text{C}$ at $10\text{ }^\circ\text{C min}^{-1}$.

Differential scanning calorimetry (DSC) was carried out on a TA Q2000 DSC using a heat-cool-heat thermal cycle. 5 mg of poly(disulfide) film was placed in an hermetic aluminum pan. The first cycle started by heating the sample from -90 to $100\text{ }^\circ\text{C}$ at $10\text{ }^\circ\text{C min}^{-1}$. The second cycle cooled the sample back to $-90\text{ }^\circ\text{C}$. The third step heated the sample again from -90 to $100\text{ }^\circ\text{C}$ at $10\text{ }^\circ\text{C min}^{-1}$.

Profilometry measurement of the photopolymerized pattern was carried out using a Dektak 150 (Bruker) profilometer.

RESULTS AND DISCUSSION

Photoinduced synthesis of poly(disulfide) network film

The ability of **XAP-TBD** to act as a photocatalyst for polymerization of polyfunctional thiols was demonstrated by irradiating continuously a thin film specimen ($1.7\text{ }\mu\text{m}$ thickness) based on trimethylolpropane tris(3-mercaptopropionate) (**3P**) with a medium-pressure Hg arc lamp ($\lambda = 200\text{--}800\text{ nm}$). After 15 min of irradiation, the **3P/XAP-TBD** mixture results in a solid transparent coating **poly3P** insoluble in a range of conventional organic solvents. **Figure 1**

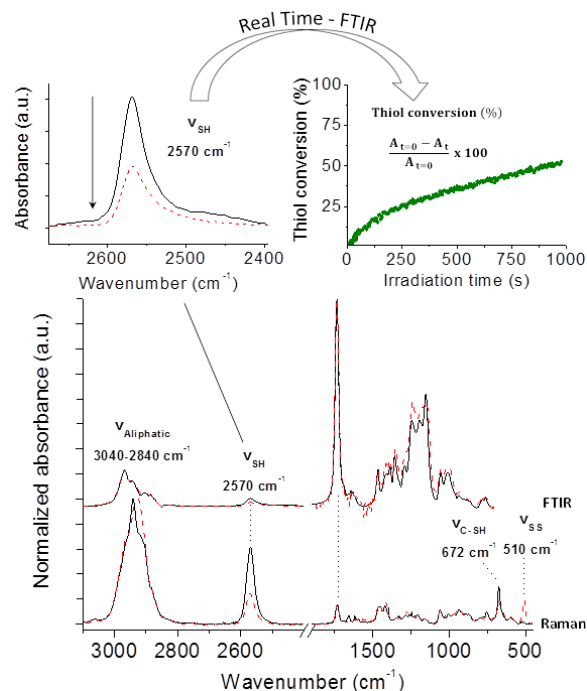


Figure 1. At the bottom, FTIR and Raman spectra of **3P** film (solid line) and **poly3P** (dashed line) after 15 min UV irradiation with non-filtered Hg-Xe medium pressure mercury vapor lamp (490 mW.cm^2). At the top, the enlarged section shows the evolution of thiol IR stretching mode at 2570 cm^{-1} (left); rapid scan analysis was exploited to obtain thiol conversion-time plot (right).

shows both the FTIR (top trace) and Raman (bottom trace) spectra before and after UV exposure. Thiol consumption is reflected by the significant decrease of the *S-H* stretching band ν_{SH} at 2570 cm^{-1} , and *C-SH* stretching band $\nu_{\text{C-SH}}$ at 672 cm^{-1} , only visible on the Raman spectrum. Similarly, the appearance of a characteristic disulfide band is only noticeable in Raman spectroscopy with the onset of a signal at 510 cm^{-1} straightforwardly attributed to the *S-S* stretching ν_{SS} . Both techniques give consistently over 50 % final thiols conversion after 15 min UV exposure (FTIR: 52 %, Raman: 51 %) calculated by integration of the SH stretching band. A conversion-time curve (at the top of Figure 1) was also obtained by synchronizing rapid-scan FTIR spectroscopy and UV exposure. It reveals that the photoinduced catalysis of the thiol oxidation to disulfide process proceeds in two stages. The first stage is characterized by fast reaction kinetics until 120 s followed by a slower stage presumably

because of mobility constraints due to high crosslink density. Note that an increase of irradiation up to 60 min eventually enabled to reach a higher conversion ($\approx 75\%$) that levels off from 40 min of irradiation (see Figure S1). To comply with conventional manufacturing methods of UV-curing demanding high throughput, a UV conveyor equipment (medium pressure mercury vapor lamp, 10 passes) was used for the cross-linking of **3P/XAP-TBD** film. Although the overall UV dose is much lower in this case (13 J cm^{-2} versus 441 J cm^{-2} in the previous case), a high energy density applied in a shorter exposure time (2.3 s) led to a conversion of 70 % from FTIR data, a value attained after much longer times ($> 40 \text{ min}$) with the first irradiation source. Our assumption is that mobility restriction may be alleviated because of both higher radical concentration and heat released (IR radiation is not filtered). In addition, this positive result emphasizes the industrial viability of this emerging UV technology having no inherent problem of oxygen inhibition in contrast to radical

photopolymerization. The ^1H NMR spectra of the **3P** monomer (trace **A**) and the insoluble **poly3P** polymer (trace **B**, solid line, obtained by solid-state MAS acquisition) were compared in **Figure 2**. The spectrum of **poly3P** displays a very broad baseline as well as wide resonances. Strongly dependent on the strength of the dipolar coupling among the protons, the significant linewidth is informative of constrained motional processes within the network. The experimental spectrum of **poly3P** was deconvoluted, and the fitted curve **B_{fit}** was superimposed on the same Figure (dotted line). A very good fitting was achieved when decomposing most proton resonances ($b'-d'$, f') with a thin and broad component showing all a similar Gaussian/Lorentzian proportion. For the sake of clarity, these two groups of thin signals (**B_{fit1}**) or broad signals (**B_{fit2}**) are shown separately. This result suggests a non-homogeneous network made of both mobile and rigid parts respectively, which is consistent with an incomplete thiol conversion.

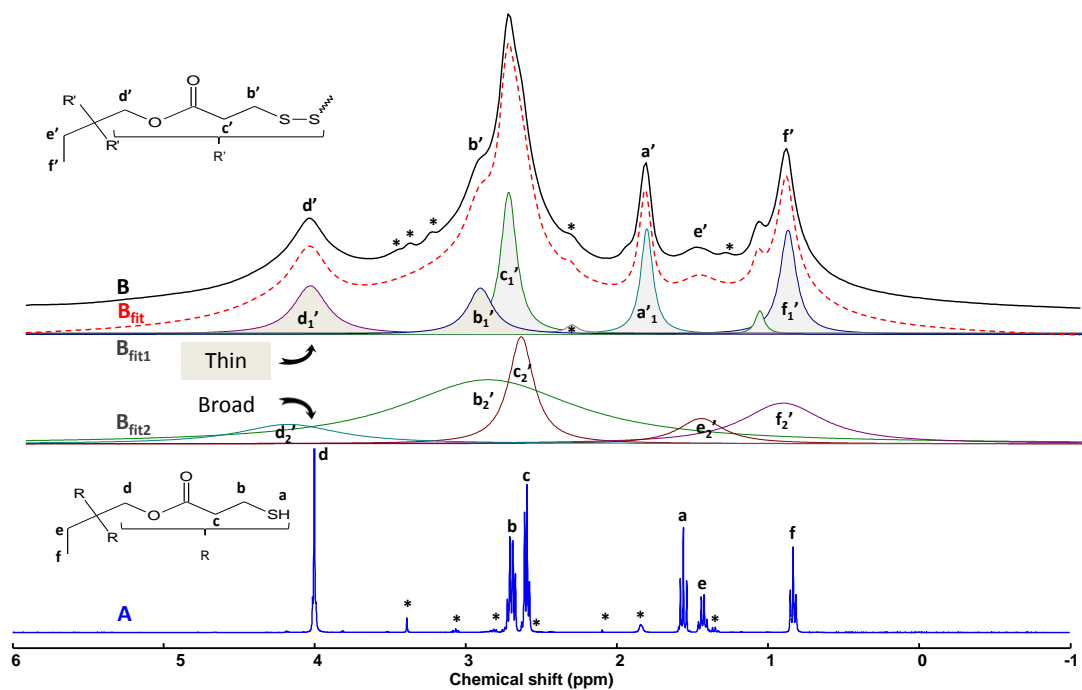


Figure 2. **A:** Liquid state ^1H -NMR spectrum of **3P**. **B:** Experimental solid state ^1H MAS NMR spectrum of **poly3P**. **B_{fit}**: simulation obtained by deconvolution of **B** with **B_{fit1}** and **B_{fit2}** gathering respectively thin and broad components. (*: impurities). Irradiation conditions: 10 passes under UV conveyor, light dose = 13.5 J cm^{-2} .

In spectrum **B**, the most significant change concerns the –SH end group protons, moving lowshield from 1.58 ppm (H_a) to 1.89 ppm (H_a'). Such shift in the polymer network may translate reduction in both self-association of thiol groups and hydrogen bonding between the thiol hydrogen and carbonyl oxygen atoms, from the liquid phase to a more rigid environment. Integration based on the deconvoluted SH proton signal (H_a') relative to the ethylenic protons ($H_{f,e'}$, 0.94–1.51 ppm) led to a conversion of 65 %, very close to FTIR data (70 %). The small discrepancy can be explained by the uncertainty resulting from the NMR spectrum's deconvolution.

Although the formation of polymer with disulfide repeating units was verified by Raman data, the exclusive formation of S–S bonds by thiol oxidation remains questionable. Short wavelength irradiation UV exposure of thiols²⁹ or the presence of strong oxidants³⁰ were found to yield sulfur species of higher oxidation states, including sulfonic acid $R-SO_3H$, thiosulfinate ($R-S(=O)-S-R$) and thiosulfonate $R-SO_2-S-R$. As a first indication, the S=O stretching band is absent from the IR or Raman spectra, but detection can be distorted by localized over-oxidation at film surface. Therefore, XPS surface analysis of the disulfide-containing polymer **poly3P** was carried out. **Figure 3** focuses on the effect of irradiation on the $S2p_{3/2, 1/2}$ spectra, while the carbon, nitrogen and oxygen spectra showed minimal variation. Deconvolution of the **3P** monomer spectrum shows the characteristic two spin-orbit pairs ($S2p_{3/2}$ and $1/2$) at 162 and 163 eV. Obviously, both the doublet structure and the binding energies are retained after photopolymerization. Only a slight signal broadening translates the change of local environment in **poly3P**. As reported for thiol self-assembly monolayers (SAMs),³¹ the XPS analysis is not able to unambiguously detect disulfide bond formation. In contrast, further oxidized sulfur species such as sulfonate or sulfinate give a distinctive contribution at binding energy of 166 eV or higher.³² A very small and broad peak arising from the noise

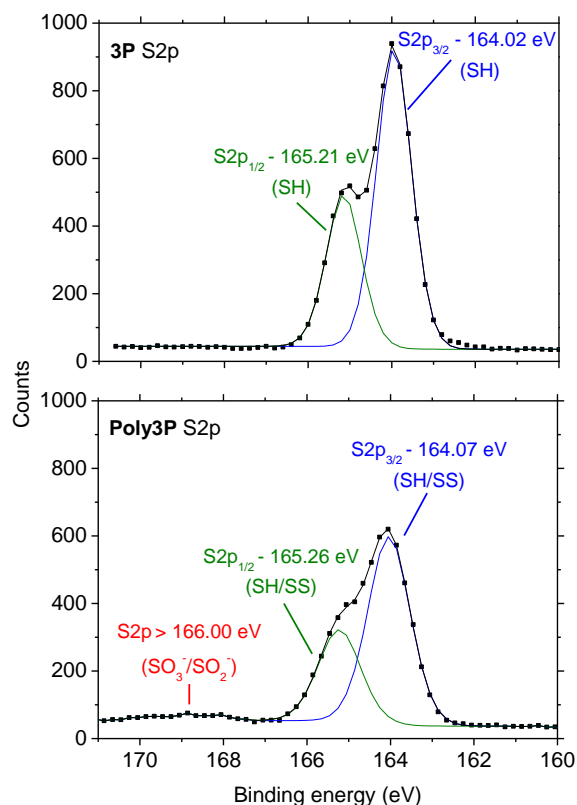
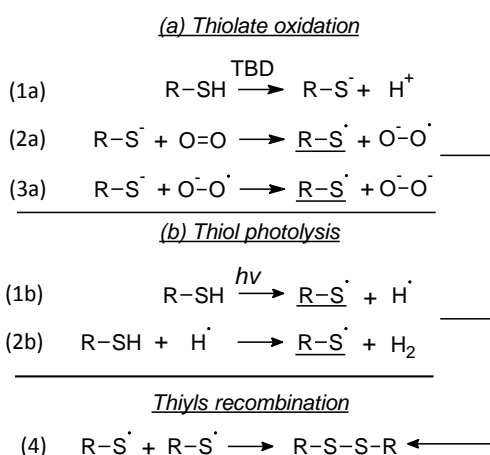


Figure 3. S2p spectra of monomer **3P** and polymer **poly3P**. Irradiation conditions: 10 passes under UV conveyor, total light dose = 13.5 J cm^{-2} , UV exposure time = 2.3 s.

level and accounting for 3 % of the sulfur atoms indicates that there is almost no over-oxidation, thereby supporting the selective and mild oxidation of thiol to disulfide. Finally, DSC analysis of **poly3P** reveals a glass transition arising at -13°C (Figure S2-A of Supporting Information SI). Such value is consistent with that of conventional poly(disulfide) elastomers.²² In addition, qualitative solubility tests have shown that **poly3P** film is chemically attacked and dissolved by a range of common organic solvents (acetone, chloroform), but only weakened in the swollen state. Such chemical resistance is related to the high sulfur content in the polymer backbone imparting insolubility.³³ However, the heat resistance remains moderate, and the TGA trace (Figure S2-B in SI) shows a thermal stability up to 170°C (2.4 % weight loss due to water evaporation) with a broad decomposition range spanning to 620°C .

Mechanism of step-growth thiol-thiol photopolymerization

Disulfide bonds can be the result of two possible reactions: recombination of two thiyl radicals, or thiyl/thiolate attack on existing S-S bonds. Consequently, S^\bullet are required to increase the disulfide concentration and form polydisulfide polymers. In our photochemical process, thiyl radicals may be generated from thiol species via two different pathways displayed in **Scheme 3**: *thiolate oxidation* (a) or/and *thiol photolysis* (b).



Scheme 3. Mechanism of disulfide bond formation by thiol irradiation via thiolate oxidation (a) or thiol photolysis (b).

Widely reported for the cross-linking of polysulfide oligomers,^{16, 34} the former involves first the formation of a thiolate intermediate species S^- (eq 1a), and its one electron oxidation by reducible species O_2 (eq 2a) or $O_2^{\bullet-}$ (eq 3a). The resultant thiyl radicals are subjected to recombination, resulting in disulfide adduct (eq 4). In addition, thiolate oxidation can be driven by the use of atmospheric oxygen (oxidant) and photogenerated TBD (catalyst). The lesser-known second reaction proceeds by a single-step photochemical decomposition of thiol groups. Its discovery dates back to 1941 by Thompson et al.³⁵ but most works in the liquid phase were undertaken by Knight in the 70s using alkyl monothiols, and consequently without concern for polymer synthesis.³⁶ In our case, the photoinduced hydrogen abstraction of

thiol may be mediated by short wavelength irradiation. Irradiation is indeed provided by unfiltered medium-pressure mercury lamps so that the emission wavelengths cover the 200-300 nm range (although the incident radiation is concentrated in the region near 254 nm) where there is a significant absorption of thiol derivatives (lamp emission spectrum and absorption spectrum of **3P** and other thiol derivatives are shown in Figure S3 and S4 of SI). Although the mechanism in solution has been poorly investigated, thiol photolysis has found a high utility as a source of hydrogen atoms, H_2 , or thiyl radicals to trigger radical photoinitiator-free thiol-ene photopolymerization for example.³⁷ In absence of molecule containing abstractable hydrogen atoms or substrate for thiyl radicals (alkene), the photolysis of thiols in liquid state is known to follow simple mechanism (Scheme 3 b) although very few data are available in the literature.³⁸ The only significant primary process is assumed to be S-H bond photocleavage (eq 1b). Two reactions of the two primary fragments, RS^\bullet and H^\bullet , can occur subsequently. H^\bullet can react with a new thiol to form H_2 and an additional RS^\bullet (eq 2b). Additionally, the two thiyl radicals can react together to form disulfide species (eq 4) or with the disulfide adduct. The likelihood of the occurrence of each identified route to form thiyl radicals has been evaluated in the following section

Thiolate oxidation

To investigate the importance of thiolate air oxidation in the disulfide bridges formation, the effect of parameters affecting both oxygen permeation into the film (atmosphere composition, film thickness) and TBD concentration ([PBG], light irradiance) was addressed. **Figure 4** depicts the thiol conversion-time curves of **3P/XAP-TBD** film under 3 different atmospheres: air, saturated oxygen and nitrogen. As mentioned previously, oxygen in the ambient air is sufficient to promote 51 % conversion after 15 min of irradiation. The yield (71 %) and oxidation rate

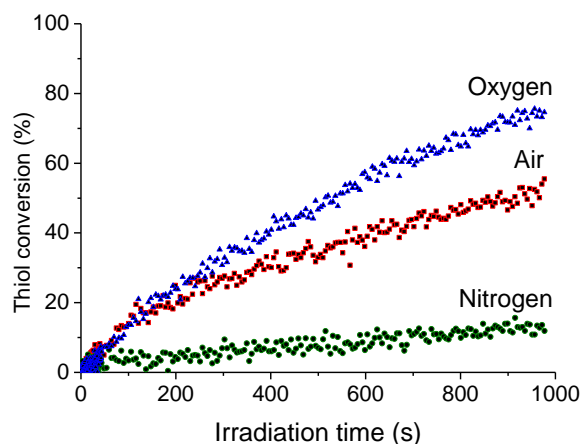


Figure 4. Thiol conversion-time plot obtained from RT-FTIR data during photopolymerization of **3P/XAP-TBD** under various atmospheres and a 15 min UV irradiation (Hg-Xe lamp, 490 mW.cm⁻²).

are both increased in an oxygen-rich environment supporting its crucial role of oxidant. In an anaerobic atmosphere (N₂), 13 % conversion is only achieved, supporting photooxidation as the dominant mechanism for the conversion of terminal thiol groups to disulfides. **Table 1** summarizes the effects of film thickness (e), PBG concentration and irradiance on thiol conversion. Kinetic profiles are clearly dependent on e in the specific range 1.9 – 7.1 μm (runs **4–8**), suggesting a regime limited by the diffusion of atmospheric oxygen. As expected by an oxidative mechanism, faster hydrolysis kinetics are obtained with thinner films promoting the entry of oxygen. Below and above these 2 threshold values, the final thiol conversions remain unchanged at 52 % (runs **1–4**, $e \leq 1.9 \mu\text{m}$) and 22 % (runs **8–10**, $e \geq 7.1 \mu\text{m}$). As expected, thiol consumption was decreased upon reducing the PBG content from 4 to 0 wt% (runs **11–13**). Above 4 wt%, a decreased efficiency was observed (runs **14–15**), however. Irradiance control the generation rate of PBG, and its value was varied from 0 to 490 mW cm⁻² (runs **16–21**). Control experiment without irradiation (run **16**) indicates that light is essential to trigger the reaction. Under irradiation, there is a progressive reactivity enhancement as the irradiance is increased.

Table 1. Effect of film thickness, concentration of **XAP-TBD** and irradiance on thiol conversion during photopolymerization of **3P/XAP-TBD** under a 15 min UV irradiation (Hg-Xe lamp, 490 mW cm⁻²).

Entry	e^a (μm)	[PBG] (wt%)	Irradiance (mW cm ⁻²)	SH conv ^b (%)
1	0.4	4	490	52
2	1			52
3	1.7			52
4	1.9			52
5	2.2			38
6	4.4			31
7	5.9			27
8	7.1			22
9	14.5			22
10	20.5			22
11	1.7	0	490	16
12		2		33
13		4		52
14		6		46
15		8		42
16	1.7	4	0	0
17			87	8
18			170	22
19			260	29
20			380	37
21			490	52

^a Film thickness. ^b Thiol conversion determined by FTIR.

Thiol photolysis

Photopolymerizations performed without PBG (run **11** in Table 1, 16 % conversion) or in a nitrogen-rich environment (Figure 4, 13 % conversion) provide a first response in favor of a concurrent non-oxidative mechanism for the formation of thiyl radicals, involving neither thiolate species nor oxidizing agent. To prove that thiol photolysis is the most reason for the formation of SS bridges under these conditions, **Figure 5** shows the effect of a filtered light on thiol conversion kinetics. Without PBG, removing the more energetic photons (λ : 330 – 450 nm) totally prevents the reaction. By contrast, irradiation with the full spectrum (λ : 200 – 450 nm) allows to convert 16 %. As expected, addition of the PBG enables to

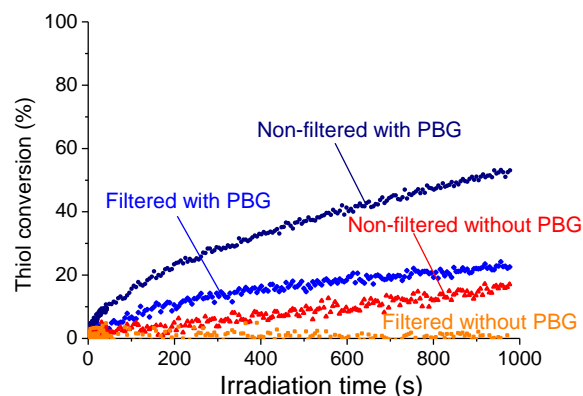


Figure 5. Thiol conversion-time plot obtained from RT-FTIR data during photopolymerization in air of **3P** under different conditions: without and with PBG **XAP-TBD** under two Hg-Xe UV irradiation settings: non filtered light ($200 < \lambda$, 490 mW cm^{-2}) and filtered light ($330 < \lambda$, 290 mW cm^{-2}).

achieve higher conversions: 23 % with a single oxidation route operating ($\lambda > 330 \text{ nm}$), and 52 % when the two photochemical mechanisms are combined ($\lambda > 200 \text{ nm}$). The higher yields obtained with the unfiltered light may result from the activation of thiol photolysis, but also from a higher PBG photolysis yield due to its apparent absorption below 330 nm (see Figure S3). Obviously, the single contribution of each mechanism is difficult to determine in this case.

Effect of thiol architecture on reactivity

Table 2 summarizes the effect of thiol functionality ($f = 2 - 4$), thiol structure (acetate: **A**, propionate: **P**) and molecular weight on final thiol conversion and glass transition temperature (T_g) for film specimens prepared under the UV-conveyor. All chemical structures are summarized in Scheme 2.

Functionality

Upon using bifunctional precursors **2P** or **2A**, yields in the order of 70 % are found. Nevertheless, these values are too low to achieve high molecular weight linear polymers and, only liquid films composed of oligomer chains were obtained after UV exposure. By contrast, film solidification occurs in other polymerizations involving thiol reactants with functionalities greater than two. In this case, a

Table 2. Characteristics of polydisulfides derived from different thiol monomers with 4 wt% of PBG **XAP-TBD** in air under UV conveyor (15 passes).

Polythiol	M_w (g mol^{-1})	SH conv. ^a (%)	T_g ($^{\circ}\text{C}$)
2A	210	73	-
2P	238	71	-
3A	357	92	6
3P	399	71	-13
4A	433	94	43
4P	489	67	19
3P₇₀₀	708	93	-27
3P₁₃₀₀	1274	100	-46

^a Thiol conversion determined by FTIR

cross-linking takes places, which is less demanding in terms of conversion than a linear step polymerization. Surprisingly, increasing f from 3 to 4 does not affect the final conversion value, averaging 70 % with propionate monomers (**3P**, **4P**) and ca. 90 % with acetate analogues (**3A**, **4A**). In contrast, there is a marked jump of 30 $^{\circ}\text{C}$ for the glass-transition, reflecting a higher cross-link density.

Thiol structure

The major change in reactivity results from the replacement of propionate to acetate: **poly3A** achieves 92 % conversion versus 71 % with **poly3P**. Consequently, polymer networks derived from acetate monomers are more tightly cross-linked resulting in T_g value approx. 20 $^{\circ}\text{C}$ higher than their analogues based on propionate. Such difference of reactivity can be interpreted in various ways. As regards route **a** (oxidation), acetate thiols have a lower pK_a value facilitating their deprotonation. Additionally, they yield a more stable acetate thiyl radical (given the proximity of electron withdrawing groups $\text{HSCH}_2\text{COO}^-$), which in the end are more likely to be oxidized.³⁹ As reported in the literature, the rate-determining step of an oxidative mechanism is not the ionic dissociation but the electron transfer from the thiolate to oxygen atom.³⁰ As regards route **b**, acetate thiol photolysis can be also facilitated by a decreased S-H bond energy in closer

proximity with the ester electron withdrawing substituent compared to propionate.

Molecular weight of thiol derivatives

The molecular weight of thiol derivatives is another critical parameter for enhancing the final conversion values. In this respect, the network derived from the two poly(ethylene oxide)-based trithiol oligomers **3P**₇₀₀ (708 g/mol) and **3P**₁₃₀₀ (1274 g/mol) showed a much higher thiol conversion (93 % and 100 %, respectively) than **poly3P** (71 %) prepared with a monomer analogue having the same functionality. Obviously, the use of thiol oligomers is accompanied by a higher PBG to SH molar ratio, which may increase reactivity. However, we noted only a limited effect of PBG concentration increase on thiol conversion (see Table 1). More importantly, thiol oligomers can impart a more mobile local environment values as demonstrated by much lower T_g values well below 0 °C. In our system, improving chain motion ability can impact positively on reaction rates because of less diffusional limitations to thiyl radicals coupling reactions and less barrier to oxygen permeation in the film (route **a**).

Towards an optimized radiation-curable thiol formulation

It is apparent that step thiol-thiol photopolymerization is a versatile means of synthesizing a host of different polydisulfide polymers starting with a single polyfunctional thiol monomer. However, very important for commercial formulations is the copolymerization of multifunctional oligomers and low-viscosity monomers, which is the cornerstone of radical or cationic radiation curing technology. By this way, the chemical structure of a polymer network can be varied over a wide range in order to obtain a product with a combination of desirable properties.

Figure 6 shows how the degree of conversion and the T_g can be modulated in a **3P/3P**₁₃₀₀ monomer/oligomer formulation containing a variable content in **3P**₁₃₀₀. A higher relative

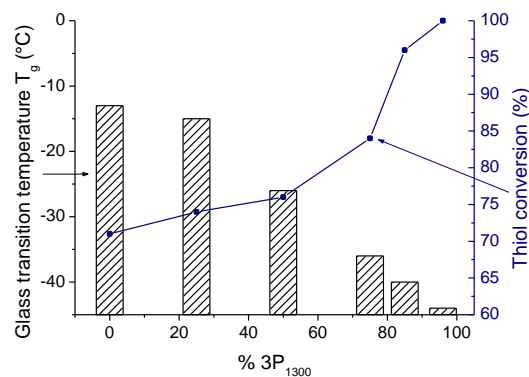


Figure 6. Glass transition temperature and thiol conversion of polydisulfide copolymer networks derived from different mixtures of **3P**₁₃₀₀ and **3P**.

fraction of **3P**₁₃₀₀ (28, 47, 78, 85 and 100 %) is marked by a gradual increase in conversion, from 74 % to 100 %, and progressive reduction of T_g values, -15 °C to -44 °C. These results suggest a more mobile network for two main reasons: the incorporation of a low T_g PEO oligomer and a lower density of crosslinks. Whatever the polymerization mechanism, thiyl radical coupling controls polymer growth. Being a diffusion-controlled reaction, its rate is strongly dependent on local chain mobility. Consequently, higher conversions can be driven by the release of mobility restriction. Upon increasing the concentration of oligomers, chain ends are no longer “frozen”, resulting in higher cure extent. Obviously, a less tightly cross-linked polymer network creates also better conditions to oxygen permeation and thiolate oxidation.

To prove the differences of molecular mobility in the polysulfide copolymers, low field NMR relaxation experiments were performed for the various cured **3P/3P**₁₃₀₀ films. It is well established that NMR transverse magnetization relaxation (T_2 relaxation) is particularly suitable for polymer network because T_2 response is highly sensitive to local constraints on large spatial scale chain mobility imposed by cross-linking.⁴⁰ Therefore, this relaxation time has proven to be an efficient probe to evaluate cross-link density, network defects and homogeneity. **Figure 7A** displays T_2 decay for a set of seven **3P/3P**₁₃₀₀ samples containing

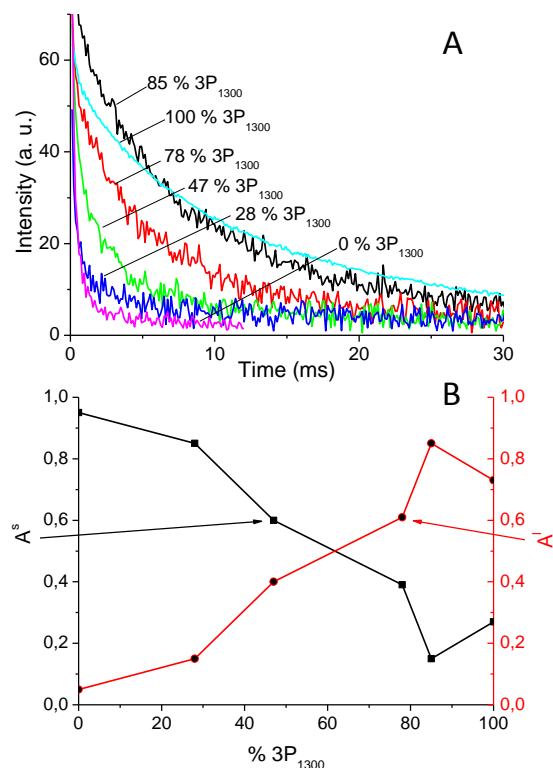


Figure 7. A. Decay of the transverse magnetization for polydisulfide copolymer network derived from **3P/3P₁₃₀₀**. B. Effect of **3P₁₃₀₀** weight concentration on fractional amplitude of the short (**A^s**, $T_2 < 0.5$ ms) and long relaxation components (**A^l**, $T_2 > 0.5$ ms).

various concentrations in **3P₁₃₀₀**. Clearly, oligomer-rich samples are characterized by a faster decaying profile, suggesting fewer constraints as regards chain motion. More quantitatively, a combination of 3 single exponential functions possessing each one a characteristic relaxation time (< 0.55 ms, 1-10 ms, 10-30 ms) are needed to obtain an accurate fitting. This observation is consistent with three different kinds of mobility in the polymer structure, and the concept of gradient mobility in a polymer network.⁴¹ Each component has a relative fraction which is proportional to the quantity of protons involved in this relaxation. For sake of simplicity, we distinguished only two populations of protons. On one hand, **A^s**, with short relaxation times (< 0.5 ms) assigned to hydrogen atoms of low mobility chain portions typically adjacent to network junctions, on the other end, **A^l**, with longer relaxation times (> 0.5 s) originating from mobile H of pendant chain ends, loosely cross-

linked networks or PBG residue. An example of fitting is shown in SI (Figure S5).

Figure 7B shows the evolution of the two relaxations components **A^s** and **A^l** with **3P₁₃₀₀** concentration. As expected, we note that the amount of glassy and immobilized polymer portion (**A^s**) decreases substantially with the concentration of oligomers. The amount of **A^s** varies from 95 % without **3P₁₃₀₀** to only 15 % in a **poly3P/3P₁₃₀₀** (15/85 %) copolymer. Surprisingly, **poly3P₁₃₀₀** does not show the lowest fraction in rigid segments (**A^s** = 27 %). In this case, a complete conversion was obtained, eliminating the contribution of mobile pendant chains formed by unreacted thiol functions.

Advanced poly(disulfide) photoresist materials via UV photolithography

Sulfur-based polymers have received considerable attention as high-n polymers, possessing a high refractive index and optical transparency. Poly(arylene sulfide)s or sulfur-containing polyimides are among the prime candidates, as they have found utility in advanced optoelectronic devices such as substrates for display devices, optical adhesives or encapsulants for antireflective coatings, and microlens.⁴⁰ Although spatial control is highly desired for the manufacture of these advanced optical devices, most synthetic routes to these polysulfide structures are not compatible with standard UV photolithography techniques using Hg vapor lamps.⁴²⁻⁴⁵ By contrast, deep UV or electron-beam lithography is more costly and require vacuum.

We show in this last section that a micrometric pattern can be photogenerated by thiol-thiol step photopolymerization with a conventional UV mask aligner (high-pressure Hg lamp) starting with a **3P₁₃₀₀/XAP-TBD** film. An optical microscopy image of the obtained photopatterned film is shown in **Figure 8A**. A cross-section image of a 150 μm -wide line pattern was analyzed by confocal Raman microscopy. A line mapping was performed, and the chemical composition (**Figure 8B**) of the

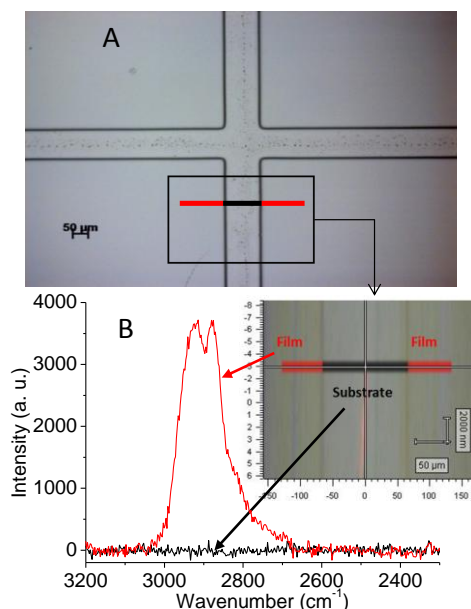


Figure 8. A. Optical microscopy image of **poly3P₁₃₀₀** photopatterned film. B. Raman mapping of the same polydisulfide film showing two regions with distinct chemical compositions: glass substrate on the central band and sulfur-polymer sample outside.

sample was determined using chemiometric analysis. Our results were consistent with the formation of two separated polydisulfide and glass substrate regions of different composition, thus suggesting the spatial control of the photopolymerization. Indeed, the irradiated regions (outside the channels) clearly show the conventional CH_2 and CH_3 vibrational modes arising from **poly3P₁₃₀₀**: ν_{CH_2} at 2852 cm^{-1} and ν_{CH_3} at 2960 cm^{-1} . A height profile was extracted from the Raman data which was compared with that obtained by profilometry measurements.

As shown in **Figure 9**, there is a good match between both physical and chemical techniques. Both profiles show well-defined edges of the pattern, and a film thickness of approximately $1.4\text{ }\mu\text{m}$. Therefore, both methods support that a good quality pattern can be photogenerated using this novel polythiol radiation curing technology.

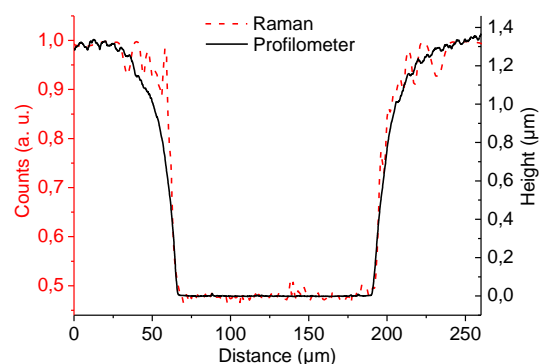


Figure 9. Height profile of a photopatterned **poly3P₁₃₀₀** films measured by Raman spectroscopy (dashed line) and profilometry (solid line).

CONCLUSIONS

A novel UV radiation curing of multifunctional thiol coatings was described. Raman, solid-state NMR spectroscopy and XPS conclusively established the almost exclusive conversion of thiols into polymer network with disulfide repeating units. Fast rates were achieved in the order of seconds with a UV conveyor. Recombination of photogenerated thiyl radicals controls the step-growth polymerization mechanism. Thiyl are predominantly formed by photobase-catalyzed thiol air oxidation, and to some extent by thiol photocleavage under short wavelength excitation ($\lambda < 300\text{ nm}$). Functionality greater than 3 is required to obtain solid films, and acetate thiols polymerize faster than equivalent propionate thiols. A more mobile network ensured by thiol oligomer incorporation enables a higher cure extent presumably because of less thiyl radical diffusional limitation. In the future, we foresee that coating properties such as adhesion, elasticity, hardness, chemical or abrasion resistance of polydisulfide films may be tailored by adjusting functionality, molecular weight and chemical structure of thiol compounds.

REFERENCES AND NOTES

1. J. G. Drobny, In *Radiation Technology for Polymers*, CRC Press: **2010**; p 307.
2. Y. Yagci, S. Jockusch, N. J. Turro, *Macromolecules* **2010**, *43*, 6245-6260.
3. S. Naumann, M. R. Buchmeiser, *Macromol. Rapid Commun.* **2014**, *35*, 682-701.

4. K. Suyama, M. Shirai, *Prog. Polym. Sci.* **2009**, *34*, 194-209.
5. T. Ishikawa. Superbases for Organic Synthesis: Guanidines, Amidines, Phosphazenes and Related Organocatalysts; John Wiley & Sons, **2009**.
6. X. Zhang, W. Xi, C. Wang, M. Podgórski, C. N. Bowman, *ACS Macro Lett.* **2016**, *5*, 229-233.
7. K. Arimitsu, R. Endo, *Chem. Mater.* **2013**, *25*, 4461-4463.
8. H. Salmi, X. Allonas, C. Ley, A. Defoin, A. Ak, *Polym. Chem.* **2014**.
9. S. Chatani, T. Gong, B. A. Earle, M. Podgórski, C. N. Bowman, *ACS Macro Lett.* **2014**, *3*, 315-318.
10. X. Sun, J. P. Gao, Z. Y. Wang, *J. Am. Chem. Soc.* **2008**, *130*, 8130-8131.
11. W. Xi, H. Peng, A. Aguirre-Soto, C. J. Kloxin, J. W. Stansbury, C. N. Bowman, *Macromolecules* **2014**, *47*, 6159-6165.
12. K. Dietliker, R. Hüsler, J. L. Birbaum, S. Ilg, S. Villeneuve, K. Studer, T. Jung, J. Benkhoff, H. Kura, A. Matsumoto, H. Oka, *Prog. Org. Coat.* **2007**, *58*, 146-157.
13. N. Feillée, A. Chemtob, C. Ley, C. Croutxé-Barghorn, X. Allonas, A. Ponche, D. Le Nouen, H. Majjad, L. Jacomine, *Macromol. Rapid Commun.* **2016**, *37*, 155-160.
14. R. P. Szajewski, G. M. Whitesides, *J. Am. Chem. Soc.* **1980**, *102*, 2011-2026.
15. J. C. Patrick. U.S. Patent 2,553,206, 1951.
16. G. B. Lowe, *J. Adhes. Adhes.* **1997**, *17*, 345-348.
17. S. Giannis, R. D. Adams, L. J. Clark, M. A. Taylor, *J. Appl. Polym. Sci.* **2008**, *108*, 3073-3091.
18. T. C. P. Lee. Properties and Applications of Elastomeric Polysulfides; Rapra Technology, 1999.
19. J.-G. Liu, M. Ueda, *J. Mater. Chem.* **2009**, *19*, 8907-8919.
20. M. Liu, S. J. Visco, L. C. De Jonghe, *J. Electrochem. Soc.* **1991**, *138*, 1891-1895.
21. M. M. Doeff, M. M. Lerner, S. J. Visco, L. C. De Jonghe, *J. Electrochem. Soc.* **1992**, *139*, 2077-2081.
22. E.-K. Bang, M. Lista, G. Sforazzini, N. Sakai, S. Matile, *Chem. Sci.* **2012**, *3*, 1752-1763.
23. B. Gyarmati, Á. Némethy, A. Szilágyi, *Eur. Polym. J.* **2013**, *49*, 1268-1286.
24. J. Canadell, H. Goossens, B. Klumperman, *Macromolecules* **2011**, *44*, 2536-2541.
25. X. Du, J. Li, A. Welle, L. Li, W. Feng, P. A. Levkin, *Adv. Mater.* **2015**, *27*, 4997-5001.
26. F. Meng, W. E. Hennink, Z. Zhong, *Biomaterials* **2009**, *30*, 2180-2198.
27. C. Decker, K. Moussa, *Makromol. Chem.* **1988**, *189*, 2381-2394.
28. D. Massiot, F. Fayon, M. Capron, I. King, S. Le Calvé, B. Alonso, J.-O. Durand, B. Bujoli, Z. Gan, G. Hoatson, *Magn. Reson. Chem.* **2002**, *1*, 70-76.
29. E. Robert-Banchereau, S. Lacombe, J. Ollivier, *Tetrahedron* **1997**, *53*, 2087-2102.
30. S. Oae, J. Doi. Organic Sulfur Chemistry; Taylor & Francis, **1991**.
31. A. L. Vance, T. M. Willey, A. J. Nelson, T. van Buuren, C. Bostedt, L. J. Terminello, G. A. Fox, M. Engelhard, D. Baer, *Langmuir* **2002**, *18*, 8123-8128.
32. D. G. Castner, K. Hinds, D. W. Grainger, *Langmuir* **1996**, *12*, 5083-5086.
33. Kishore, K.; Ganesh, K., In Polymers containing disulfide, tetrasulfide, diselenide and ditelluride linkages in the main chain, Springer: **1995**; p 81-121.
34. E. Q. Rosenthal, J. E. Puskas, C. Wesdemiotis, *Biomacromolecules* **2011**, *1*, 154-164.
35. N. Skerrett, N. Thompson, *Trans. Faraday Soc.* **1941**, *37*, 81-82.
36. D. D. Carlson, A. R. Knight, *Can. J. Chem.* **1973**, *51*, 1410-1415.
37. N. B. Cramer, J. P. Scott, C. N. Bowman, *Macromolecules* **2002**, *35*, 5361-5365.
38. Knight, A. R., In Photochemistry of thiols, John Wiley & Sons, Ltd.: **1974**; pp 455-479.
39. M. Hong, S.-R. Liu, B.-X. Li, Y.-S. Li, *J. Polym. Sci., Part A: Polym. Chem.* **2012**, *50*, 2499-2506.
40. V. M. Litvinov, A. A. Dias, *Macromolecules* **2001**, *34*, 4051-4060.
41. A. Papon, K. Saalwachter, K. Schaler, L. Guy, F. Lequeux, H. Montes, *Macromolecules* **2011**, *44*, 913-922.
42. M. Caddy, T. J. Kemp, *Eur. Polym. J.* **2003**, *39*, 461-487.
43. L. Feller, J. P. Bearinger, L. Wu, J. A. Hubbell, M. Textor, S. Tosatti, *Surf. Sci.* **2008**, *602*, 2305-2310.
44. J.-G. Liu, Y. Nakamura, T. Ogura, Y. Shibasaki, S. Ando, M. Ueda, *Chem. Mater.* **2008**, *20*, 273-281.
45. M. Hirata, Y. Abe, B. Ochiai, T. Endo, *J. Polym. Sci., Part A: Polym. Chem.* **2010**, *48*, 4385-4392.